2023 Fourth International Symposium on 3D Power Electronics Integration and Manufacturing (3D-PEIM) | 978-1-6654-9967-5/23/$31.00 ©2023 IEEE | DOI: 10.1109/3D-PEIM55914.2023.10052332

Laser-induced graphene supercapacitors on flex substrates for package-integrated power supply

Reshmi Banerjee*
Biomedical Engineering
Florida International University
Miami, USA
rbane003@fiu.edu

Azmal Huda Chowdhury*
Mechanical and Materials Engineering
Florida International University
Miami, USA
achow030@fiu.edu

Pavar Sai Kumar
MEMS, Microfluidics and Nanoelectronics Lab
Birla Institute of Technology and Science Hyderabad Campas,
Hyderabad, India
p20200440@hyderabad.bits-pilani.ac.in

Chunlei Wang
Mechanical and Materials Engineering
Florida International University
Miami, USA
wangc@fiu.edu

Sanket Goel
MEMS, Microfluidics and Nanoelectronics Lab
Birla Institute of Technology and Science Hyderabad Campas,
Hyderabad, India
sgoel@hyderabad.bits-pilani.ac.in

Pulugurtha Markondeya Raj
Biomedical Engineering
Florida International University
Miami, USA
mpulugur@fiu.edu

*Authors contributed equally

***Abstract*—Integrated power sources have a critical role in the operation of miniaturized, lightweight, wearable medical and IoT devices. Such power sources should be ideally grown directly on the package substrates for low-impedance power delivery and assembled in planar architectures while also achieving higher power densities. This paper shows laser-induced graphene supercapacitors on flexible packages to address that critical need. With the proper selection of laser wavelength and power, polyimide can be selectively transformed into porous graphene to form high surface area electrodes. These graphene layers are integrated with copper tape to a stainless-steel substrate to form planar supercapacitor layers. Initial testing was performed with liquid electrolytes. Capacitance densities of 1.2 mF/cm^2, comparable to current porous graphene capacitors but with a simpler process, was thus achieved. This unique nanomanufacturing paradigm can broadly benefit all future power module integration strategies.**

Keywords—supercapacitors, graphene, laser-induced graphene

I. INTRODUCTION

With the general trend towards the miniaturization of electronic devices, primarily for the Internet of Things (IoT) and wearable medical device applications, there is a growing demand for reliable in-package energy and power sources. Such tiny modules are expected to occupy a footprint of no more than a few cm^2 so that they can be easily integrated into system packages while manufactured using approaches compatible with prevalent substrate technologies. They are designed to provide power in the range of several μW to hundreds of mW and energy in the range of several hundreds of μWh to several mWh, suitable for running wearable and flexible health-monitoring units[1-3] that typically consist of wearable electrochemical sensors [4], energy harvesters [5], and others. Other than wearable devices, recent concentration on energy storage devices has seen a considerable boost due to the evolution of the electric vehicles. This sector concentrates on batteries, supercapacitors, and fuel cells, creating the need for novel materials synthesis with high surface area and stability [6-10].

The key focus of this paper is to advance power sources for applications in wearable devices and IoT sensor nodes. The power is typically supplied through wireless telemetry using inductive or RF links [11]. Alternatively, power can also be generated from miniaturized energy harvesters. A key element of power delivery is energy storage through various electrochemical Energy Storage (EES) devices such as micro batteries, and micro-supercapacitors, which have been continually enhanced in the last two decades to store the energy at higher densities and respond appropriately at peak power demand [12]. Among batteries and supercapacitors, the latter has the advantage of fast charge-discharge, high power densities, and smaller energy capacities than batteries [11-14]. Therefore, for low-power sensor nodes, supercapacitors are a better choice for applications such as sensor and IoT nodes. All-solid-state rolled-up supercapacitors with a capacitance density of 448 mF/cm^2 at a scan rate of 10 mV/s with a density of 9.49

978-1-6654-9967-5/23/$31.00 ©2023 IEEE

mg/cm^2 were recently shown to continuously power green LED (Light emitting diodes) for 20 s [15].

Supercapacitors can be classified as electric double-layer capacitors (EDLC) and pseudo supercapacitors. Although pseudocapacitors can achieve higher energy capacitance, the cyclability is limited due to the redox reactions that form the key feature of batteries. On the other hand, due to the simple working mechanism of the EDLCs, they can operate through thousands of cycles without significant performance degradation.

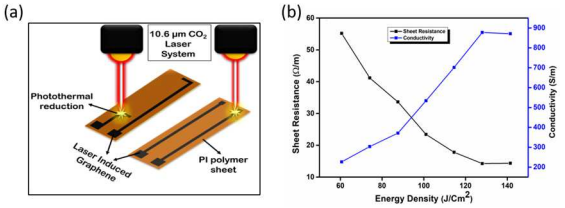

Fig.1 Sheet Resistance vs Conductivity of Laser Induced Graphene (LIG)

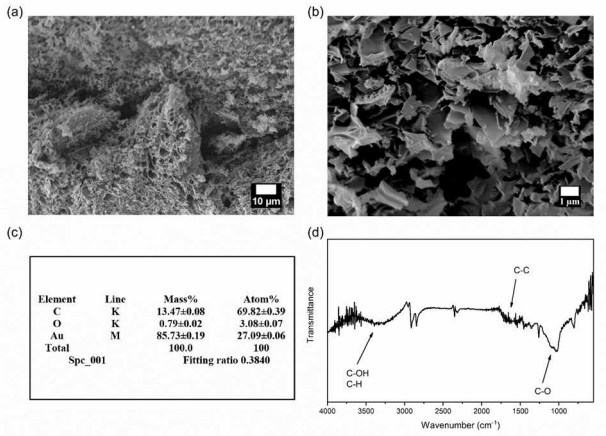

Fig. 2 (a), (b) SEM images of Laser Induced Graphene (LIG) electrodes (b) Energy Dispersive Spectroscopy (EDS) analysis (d) FTIR spectrum of LIG

To achieve higher capacitance from the electrode/electrolyte interfaces, EDLCs should use electrodes with high surface area. Over recent years, various 1D and 2D nanomaterials such as carbon nanotubes (CNTs) and graphene have been employed to achieve high areal capacity from the EDLCs [11, 13]. Among these, graphene has shown superiority due to its high surface area and electrical conductivity, which are characteristics of a good electrode material [12, 14]. However, commercial synthesis of graphene involves costly and environmentally harmful processes [15, 16]. In order to address this shortcoming, recently, low-cost laser-induced graphene (LIG) has been shown as a promising method to realize high-quality graphene on a flexible polymer such as polyimide [12, 15, 16]. For instance, a recent study shows LIG-based supercapacitor achieved capacitance densities of 44 mF/cm^2, with conductivities of 5-25 S/cm, and power densities of 9 mW/cm^2 [16]. In this paper, energy storage is achieved through a thin-film micro-fabricated supercapacitor from laser-induced graphene-based planar electrodes and liquid electrolytes. The component properties demonstrated through this work are projected to achieve high power levels with ultra-thin form-factors and easier integration with the flexible system substrates.

II. Experimental Section

A. Laser Induced Graphene

Polyimide (PI) films (0.2-0.4 mm, McMaster-Carr) are scribed with a CO_2 infrared laser. The fundamental electrode structure and design is initially created using CorelDRAW. A laser engraver and cutter is used for the synthesis of porous conductive patterned Laser Induced Graphene (LIG) electrodes. Specifically, a CO_2 laser system (Universal Laser Systems, Version 3.6) with 10.6 μm wavelength, maximum power 30W and maximum speed of 2500 mm/s was utilized for the run. The sheet resistance and conductivity typically depend on the laser energy density. Fig. 1 shows the synthesis process and typical LIG performance curve for the CO_2 laser. The ideal laser parameters of 9.5 % of maximum power and 4.5 % of maximum speed were selected to achieve high conductivity within the tool power constraints.

B. Material Characterization

The morphology of the LIG was observed and analyzed using Scanning Electron Microscopy (SEM), Energy Dispersive Spectroscopy (SEM-EDS) (Jeol FS100), and Fourier Transform Infrared Spectroscopy (FTIR) (JASCO FT/IR 4100). The LIG sample is sputtered with a gold coating for image acquisition and analysis. Fig. 2a and Fig.2b display the typical porous

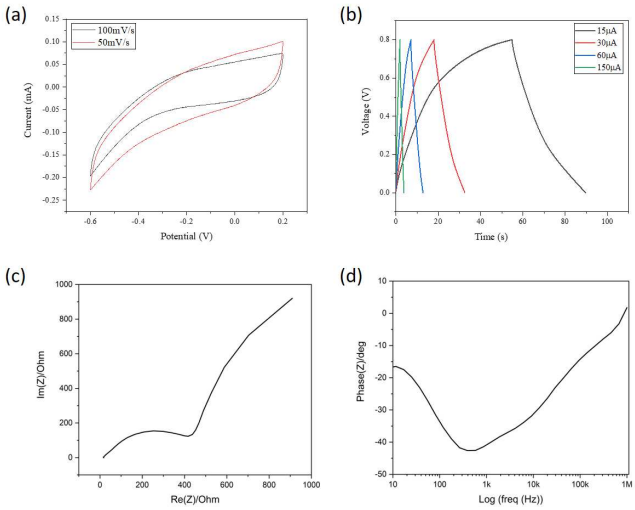

Fig.3 Electrochemical Characterization of supercapacitic behavior of porous LIG electrodes (a) Cyclic Voltammograms (b) Global Charge-Discharge (c), (d) EIS measurements

morphology of graphene. Multiscale pore structure is observed with the larger pores to be of approximately 4 microns. Fig. 2c shows the results of eelemental characterization performed using SEM-Energy Dispersive spectroscopy (SEM-EDS), indicating the presence of only carbon and oxygen other than the sputtered gold. However, EDS may be considered unreliable for accurate quantification of elements with atomic numbers below 11. FTIR analysis was additionally performed for accurate material characterization by identifying the chemical functional

groups present in the LIG samples. The broad absorption peak around 3340 cm^{-1} seen in Fig. 2d indicates the presence of hydroxyl (OH) groups. Additionally, peaks detected at 1600 cm^{-1} and 1430 cm^{-1} are attributed to aromatic C═C stretching and C-H bending, respectively. The peaks at around 1330 cm^{-1} and 1040 cm^{-1} are ascribed to C-O stretching bonds as seen in Fig. 2d. The presence of these functional groups shows that the deposited material is mostly GO.

C. Supercapacitor Fabrication

In order to fabricate the supercapacitor devices, two electrodes, are mounted on two glass slides using a conductive copper tape. The electrodes are assembled face-to-face and are separated by a thin layer of commercially available microporous polypropylene (Celgard 2400) separator soaked in 1 M of Sodium Sulfate (Na_2SO_4) solution, which allows ion exchange. The wires soldered to the two ends serve as the points of contact for the electrochemical characterization studies. The entire device was sealed using a Polyimide (Kapton®) tape.

D. Electrochemical Characterization

The electrochemical characterization was carried out in a two-electrode configuration using VMP-3 Multichannel Potentiostat (Biologic, France). A symmetric cell configuration consisting of two LIG electrodes is adopted for electrochemical analysis. One mol/L Na_2SO_4 solution is used as the electrolyte for all the characterization. Time domain cyclic voltammetry (CV), galvanostatic charge-discharge (GCD), and frequency-domain electrochemical impedance spectroscopy (EIS) were performed to investigate the electrochemical performance and double layer capacitance of the symmetric cell. Fig 3c, d show the spectral measurements (EIS) obtained from 1MHz to 1mHz. The CV and GCD were carried out in the voltage window of 0-0.8V as seen in Fig 3a and 3b. The cyclic voltammetry study is carried out at two different scan rates of 50 mVs^{-1} and 100 mVs^{-1} whereas the GCDs study is pperformed at 15µA, 30µA, 60µA, and 150µA current loadings.

III. RESULTS AND DISCUSSION

The LIG electrodes were systematically written on to the commercially available Polyimide (PI) sheet through photothermal reduction process [12, 17]. Fig. 1 shows the schematic of LIG synthesis process. The synthesis process used a commercially available CO_2 laser system to pattern the desired shapes on the PI sheet. At an optimized power of 1.95 W and 112.5 mm/s working speed, the obtained LIG was high in quality as evident from our reported work [17, 18]. The localized temperatures (> 2500 °C), created during the irradiation onto the PI, breaks down the C-O, C=O, and C-N bonds allowing the quick rearrangements leading to form the graphitic structures. The repeating units of imide and aromatic rings in the PI were leveraged to form LIG [19]. The obtained LIG was thoroughly characterized for its structural and chemical information as per our previous reports [20, 21].

The unique structure of the LIG has prospects for application in energy storage devices. In this present study, the LIG was used to fabricate symmetric supercapacitors as a promising energy storage device for wearable electronics. All the electrochemical parameters were normalized with the geometric footprint area of the electrodes. Figure 3a shows the CV profiles of the LIG-based supercapacitor. The CV profiles feature almost rectangular shapes at different scan rates, which indicates an ideal electric double layer capacitor (EDLC) behavior. The cyclic profile shows perfect symmetry with respect to the zero-y-axis , thereby illustrating excellent reversibility of the device. The average capacitance can be estimated from the CV measurements using the following formula:

$$C = \frac{1}{2v\Delta V} \int i(V)dV \qquad (1)$$

where v is the scan rate in Volts/second, V is the applied potential in Volts, and i the current in Amperes, and is estimated using the area under the curve. The figure shows that the capacitive behavior decreases with increasing scan rate, a typical behavior of EDLCs. The capacitance was estimated to be 1.17mF/cm^2 ~ 1.2mF/cm^2 for the scan rate of 50mV/s. The galvanostatic charge-discharge (GCD) studies were also carried out to further study the electrochemical characteristics of the LIG supercapacitor (Figure 3b). Again, the performance shows symmetric and linear GCD curves with negligible ohmic loss.

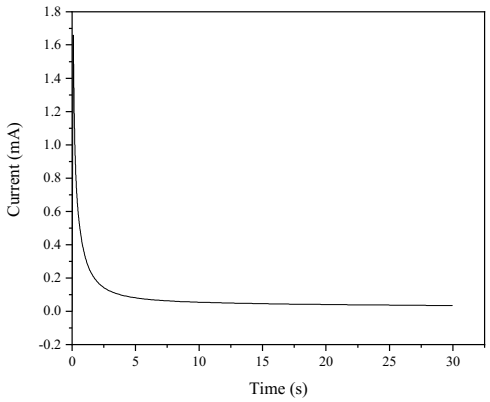

Fig.4 Rapidly decaying current in LIG

The average areal capacitance of the device can also be calculated from the GCD using the following formula:

$$C = \frac{1}{\Delta V} \int i_{d_c}\, dt \qquad (2)$$

Where i_{dc} is the discharge current and V is the voltage window of 0.8V. The real capacitance at 1.5 x 10^{-5} A was estimated to be 1.27mF/cm^2. The estimated values of capacitance density using cyclic voltammetry and galvanostatic charge-discharge are comparable. The high value of capacitance can be attributed to the highly porous morphology of the LIG. Additionally, the effect of mass loading on the capacitance of the devices need to investigated in the future. Fig. 3c shows the Nyquist plot, which is a complex-plane representation of real versus imaginary part of impedance. The EIS analysis shows that the charge transfer resistance is ~400 Ohm, which is consistent with the high conductivity from the LIG for energy storage devices.

Additionally, the Bode plot, representing impedance phase angle as a function of frequency is depicted in Fig. 3d. The capacitive behavior is visible in the low frequency range, whereas the specimens display resistive behavior at higher frequencies. Because of the high series resistance, the phase angle doesn't reach below -40° and the device is not purely capacitive as anticipated. The electrolyte is observed to have a low resistance and suitable for integrating energy storage devices. Additionally, the chronoamperometry studies showed the capacitive current, which decayed rapidly at the onset of a potential of 0.8 V. The capacitive (rapidly decaying) current, depicted in Fig. 4, is observed due to the migration of the electrochemically active species (ion flux) to the electrode surface due to the potential difference. The LIG supercapacitor approach thus demonstrated in this paper also allows easier integration into flexible electronics as polyimide is the most common substrate material in such applications. Alternative supercapacitor configurations based on interdigitated electrodes and incorporation of solid electrolytes will also extend the applicability of this technology into broader application space. The laser-based direct-write approach can be extended to seamlessly integrate the power sources with other system components such as power conditioning devices, sensing electrode and wireless communication interfaces.

IV. Conclusions

Laser-induced graphene fabrication process was developed and utilized for realizing electric double layer supercapacitors. This one-step synthesis process of graphene from commercial polyimide and laser engraver is demonstrated to be a convenient and cost-effective approach for energy storage devices due to the higher accessible surface area. Electrochemical analysis showed that the electrodes can achieve high capacitance of ~1.27 mF/cm^2 at a discharge current of 0.15 μA. Further enhancements in porous LIG supercapacitors are required to achieve higher capacitance density and lower power delivery impedance through smaller electrode resistances. This can be achieved by optimizing the LIG fabrication parameters including alternative polymer substrates as well as optimum power settings to obtain more conductive and porous graphene electrodes.

V. Acknowledgement

The authors would like to acknowledge funding support from the National Science Foundation (NSF) awards 2126190 and 2107318, as well as Precise Advanced Technologies and Health Systems for Underserved Population Engineering Research Center (PATHS-UP ERC).

References

[1]B. Jafarizadeh, A. H. Chowdhury, I. Khakpour, N. Pala, and C. Wang, "Design Rules for a Wearable Micro-Fabricated Piezo-Resistive Pressure Sensor," Micromachines, vol. 13, no. 6, 2022, doi: 10.3390/mi13060838.

[2]A. H. Chowdhury, I. Khakpour, B. Jafarizadeh, N. Pala, and C. Wang, "A Facile Fabrication of Porous and Breathable Dielectric Film for Capacitive Pressure Sensor," in 2020 IEEE SENSORS, 25-28 Oct. 2020 2020, pp. 1-4, doi: 10.1109/SENSORS47125.2020.9278604.

[3]A. H. Chowdhury, B. Jafarizadeh, N. Pala, and C. Wang, "Wearable Capacitive Pressure Sensor for Contact and Non-Contact Sensing and Pulse Waveform Monitoring," Molecules, vol. 27, no. 20, doi: 10.3390/molecules27206872.

[4]Y. Yang et al., "A laser-engraved wearable sensor for sensitive detection of uric acid and tyrosine in sweat," Nature Biotechnology, vol. 38, no. 2, pp. 217-224, 2020/02/01 2020, doi: 10.1038/s41587-019-0321-x.

[5]Y. Yu et al., "Biofuel-powered soft electronic skin with multiplexed and wireless sensing for human-machine interfaces," Science Robotics, vol. 5, no. 41, p. eaaz7946, 2020/04/22 2020, doi: 10.1126/scirobotics.aaz7946.

[6]M. Zhang, Y. Shan, Q. Kong, and H. Pang, "Applications of metal–organic framework–graphene composite materials in electrochemical energy storage," FlatChem, vol. 32, p. 100332, 2022/03/01/ 2022, doi: https://doi.org/10.1016/j.flatc.2021.100332.

[7]M. S. I. Sozal et al., "Electrical, thermal, and H2O and CO2 poisoning behaviors of PrNi0.5Co0.5O3-δ electrode for intermediate temperature protonic ceramic electrochemical cells," International Journal of Hydrogen Energy, vol. 47, no. 51, pp. 21817-21827, 2022/06/16/ 2022, doi: https://doi.org/10.1016/j.ijhydene.2022.05.011.

[8]S. Das et al., "Synthesis and flash sintering of zirconium nitride powder," Journal of the American Ceramic Society, https://doi.org/10.1111/jace.18421 vol. 105, no. 6, pp. 3925-3936, 2022/06/01 2022, doi: https://doi.org/10.1111/jace.18421.

[9]A. Nazir, H. T. T. Le, A.-G. Nguyen, J. Kim, and C.-J. Park, "Conductive metal organic framework mediated Sb nanoparticles as high-capacity anodes for rechargeable potassium-ion batteries," Chemical Engineering Journal, vol. 450, p. 138408, 2022/12/15/ 2022, doi: https://doi.org/10.1016/j.cej.2022.138408.

[10]A. Nazir, H. T. T. Le, A. Kasbe, and C.-J. Park, "Si nanoparticles confined within a conductive 2D porous Cu-based metal–organic framework (Cu3(HITP)2) as potential anodes for high-capacity Li-ion batteries," Chemical Engineering Journal, vol. 405, p. 126963, 2021/02/01/ 2021, doi: https://doi.org/10.1016/j.cej.2020.126963.

[11]C. Buch et al., "Ultra-Thin Wireless Power Module with Integration of Wireless Inductive Link and Supercapacitors," in 2016 IEEE 66th Electronic Components and Technology Conference (ECTC), 31 May-3 June 2016 2016, pp. 2364-2371, doi: 10.1109/ECTC.2016.318.

[12]J. Lin et al., "Laser-induced porous graphene films from commercial polymers," Nature Communications, vol. 5, no. 1, p. 5714, 2014/12/10 2014, doi: 10.1038/ncomms6714.

[13]I. Khakpour, A. Rabiei Baboukani, A. Allagui, and C. Wang, "Bipolar Exfoliation and in Situ Deposition of High-Quality Graphene for Supercapacitor Application," ACS

Applied Energy Materials, vol. 2, no. 7, pp. 4813-4820, 2019/07/22 2019, doi: 10.1021/acsaem.9b00479.

[14]A. F. Sardinha, D. A. L. Almeida, and N. G. Ferreira, "Electrochemical impedance spectroscopy correlation among graphene oxide/carbon fibers (GO/CF) composites and GO structural parameters produced at different oxidation degrees," Journal of Materials Research and Technology, vol. 9, no. 5, pp. 10841-10853, 2020/09/01/ 2020, doi: https://doi.org/10.1016/j.jmrt.2020.07.082.

[15]Y. Liu et al., "High-Performance Flexible All-Solid-State Supercapacitor from Large Free-Standing Graphene-PEDOT/PSS Films," Scientific Reports, vol. 5, no. 1, p. 17045, 2015/11/20 2015, doi: 10.1038/srep17045.

[16]Z. Wan, X. Chen, and M. Gu, "Laser scribed graphene for supercapacitors," Opto-Electronic Advances, vol. 4, no. 7, pp. 200079-1-200079-21, 2021/07/25 2021, doi: 10.29026/oea.2021.200079.

[17]P. S. Kumar, K. Gohel, and S. Goel, "Graphenized Papertronic Devices using Blue Laser ablated Polyimide Resin Paper," in 2021 IEEE 16th Nanotechnology Materials and Devices Conference (NMDC), 12-15 Dec. 2021 2021, pp. 1-4, doi: 10.1109/NMDC50713.2021.9677540.

[18]A. Kothuru, C. H. Rao, S. B. Puneeth, M. Salve, K. Amreen, and S. Goel, "Laser-Induced Flexible Electronics (LIFE) for Resistive, Capacitive and Electrochemical Sensing Applications," IEEE Sensors Journal, vol. 20, no. 13, pp. 7392-7399, 2020, doi: 10.1109/JSEN.2020.2977694.

[19]S. Dudala, S. K. Dubey, A. Javed, A. Ganguly, and S. Goel, "Electromicrofluidic device with integrated PDMS microchannel and laser-induced graphene electrodes for electrochemical detection of cardiac biomarker in a point-of-care platform," Journal of Micromechanics and Microengineering, vol. 32, no. 10, p. 104001, 2022/08/31 2022, doi: 10.1088/1361-6439/ac8a55.

[20]M. D. Wagh, H. R, P. S. Kumar, K. Amreen, S. K. Sahoo, and S. Goel, "Integrated Microfluidic Device With MXene Enhanced Laser-Induced Graphene Bioelectrode for Sensitive and Selective Electroanalytical Detection of Dopamine," IEEE Sensors Journal, vol. 22, no. 14, pp. 14620-14627, 2022, doi: 10.1109/JSEN.2022.3182293.

[21]P. Rewatkar, A. Kothuru, and S. Goel, "Laser-induced Flexible Graphene Bioelectrodes for Enzymatic Biofuel Cell," in 2019 IEEE 13th International Conference on Nano/Molecular Medicine & Engineering (NANOMED), 21-24 Nov. 2019 2019, pp. 30-34, doi: 10.1109/NANOMED49242.2019.9130617.